

Modeling the formation of stylolites in sedimentary rocks.

A. Rolland¹, R. Toussaint¹, P. Baud¹, J. Schmittbuhl¹, N. Conil², D. Koehn³, F. Renard⁴, J.P. Gratier⁴

Abstract. Stylolites are ubiquitous pressure solution seams found in sedimentary rocks. Analyzing the scaling properties of their height over their average direction shows that at small scale, these are self affine surfaces with a Hurst exponent around 1, and at large scale, they follow another self affine scaling with Hurst exponent around 0.5. We present how the dissolution reaction rate is affected by the deviation between the principal stress axis, and the local interface between the rock and the soft material in the stylolite. The free energy entering in the dissolution reaction kinetics is expressed from the surface energy term, and via integration from the stress perturbations due to these local misalignments. The resulting model for the interface evolution is shown, when the largest principal stress is normal to the interface, as for a stylolite, to consist of two stabilizing terms, a surface energy one dominant at small scale, and an elastic one dominant at large scale. Integrating in the model the presence of small scale heterogeneities associated to the rock grains, leads to the formulation of a Langevin equation for the dynamic surface evolution model. This equation leads to saturated surfaces obeying the two observed scaling laws. Studying it analytically and numerically, one shows that the cross over length separating the two scaling regimes directly depends on the imposed far field stress magnitude. Hence, this method proposes the basis of development of a paleostress magnitude marker. The method is next applied to stylolites found in the limestones from the logs of Bure-sur-Meuse. The practical determination of paleostresses is illustrated on this example.

1. Introduction

In recent papers, stylolites are presented as fossilized signatures of the stress field [Ebner *et al.*, 2008, 2010a]. These geologic structures are rough pressure-solution features that sprawl over the micrometric size, sometimes up to hundredth of meters. Bathurst [1987] describes stylolites as serrated interfaces between two rock masses with an amplitude greater than the diameter of the transected grains giving a sutured appearance. He makes a difference with dissolution seams or 'flaser' which are smooth, undulating, lacking in sutures and fitting around grains instead of cutting through them. Stylolites are most often found in carbonates [Stockdale, 1922, 1926, 1936, 1943; Dunnington, 1954; Bushinskiy, 1961; Park and Schot, 1968; Bathurst, 1971; Buxton and Sibley, 1981; Railsback, 1993] but also in sandstones [Young, 1945; Heald, 1955], shales [Wright and Platt, 1982; Rutter, 1983], cherts [Bushinskiy, 1961; Iijima, 1979; Cox and Whitford-Stark, 1987] and sometimes in coal [Stutzer, 1940]. Stylolites are flat at the first order, usually perpendicular to the maximum principal stress at the time of their formation (weight of the overburden or maximum tectonic stress). They are normally filled with insoluble material such as clay particles, oxides and organic matters. They are divided in two groups according to their orientation with respect to the bedding of the surrounding rock or to the orientation of their

'teeth' with respect to the mean plane of the stylolite. The stylolites of the second group are called 'slickolites' [Ebner *et al.*, 2010a]. These develop when there is a preferential plane for their growth (bedding or crevice). In this case, the stress is not perpendicular to the mean plane of the stylolite [Stockdale, 1922], but the teeth sides are subparallel to the maximum principal stress axis. The first group shows two types of orientation: sedimentary stylolites which are parallel to the bedding plane and formed under the lithostatic pressure and tectonic stylolites which are oblique or even perpendicular to the bedding, depending on the maximum tectonic stress. The teeth orientation is in all cases an indicator of the direction of the major principal stress. Benedicto and Schultz [2010] investigated the topography of stylolites (along-strike trace length, maximum and average amplitudes) from the damaged zone of the Gubbio normal fault zone in central Italy. They showed that the amount of contractional strain accommodated by stylolites as well as their length and their number increase according to the topography parameters. Analysis of cores from boreholes reveal also an increase in stylolite abundance with depth [Lind, 1993]. Fabricius and Borre [2007] compared formation of chalk from boreholes on the Ontong Java Plateau and in the central North Sea. They showed that the burial stress and the temperature play distinct roles in the burial diagenesis and porosity development of chalk. Pressure dissolution and physical compaction are controlled by the burial stress while the temperature controls recrystallization and cementation. Moreover Lind [1993] suggests that mineralogical anomaly is an initializing factor in stylolite formation such as burrows, shale clasts or flaser structures.

Only few papers report experiments about stylolites formation. Indeed, they are inherently difficult to reproduce as the kinetics of pressure-solution processes is very slow [Rutter, 1976]. Field studies [Park and Schot, 1968; André, 2003] suggest that many parameters play an important role in their development such as confining pressure, deviatoric stress, fluid pressure, temperature, shape and assemblage of

¹Institut de Physique du Globe, Université de Strasbourg, France

²ANDRA, Bure, France

³School of Geographical and Earth Sciences, University of Glasgow, UK

⁴IsTerre, University of Grenoble, France

grains, anisotropy of minerals, rates of solution, etc.. Experiments were conducted either on aggregates [Cox and Paterson, 1991; Renard et al., 2001; Gratier et al., 2005] or with indenter techniques [Gratier and Guiguet, 1986; Gratier, 1993; Gratier et al., 2004; Dysthe et al., 2002; D.K. et al., 2003]. Dysthe et al. [2002]; D.K. et al. [2003] used an indenter technique in which a Sodium Chloride crystal was kept in contact with a piston at a given pressure and temperature for several months. A fluid at compositional equilibrium with the crystal is trapped between the sample and the indenter. The contact was seen to evolve due to pressure solution during the indentation, and an Andrade creep law was shown to control the indentation rate. The evolving microstructures in the contact seemed different from stylolites. Gratier et al. [2004] used a similar technique in which a sample of Bure argillite was kept in contact with a piston, with a saturated brine in the contact, at an imposed pressure and temperature for several months. No evidence of pressure-solution was observed in this case. Karacz et al. [2008] loaded a halite cone-shaped indenter against a flat silicate surface immersed in an undersaturated brine. Using confocal microscopy techniques, they observed that the evolution of the system is dictated by an interaction between two deformation mechanisms: undercutting dissolution reducing the area of the contact and plastic flow increasing it. Recently, similar experiments were carried out with a brine at chemical equilibrium with the crystal Laronne Ben-Itzhak et al. [2012a], and emerging evolving islands and channels were observed in the contact. Such island and channels structures was first observed in the contacts during experiments on aggregates Schutjens and Spiers [1999]; Den Brok and Spiers [1991]).

Other experiments on aggregates were carried out by Gratier et al. [2005]. They loaded layers of fine quartz sand grains. The experiment lasted several months at 350 C, under 50 MPa of differential stress and in presence of an aqueous silica solution. Microstylolites were observed for the first time in the laboratory to be created at the stressed contacts between the quartz grains. Den Brok and Morel [2001] loaded elastically K-alum crystals at a controlled temperature and in a saturated K-alum solution. A hole was drilled in the middle of the crystals to provide an elastic strain gradient. They observed macroscopic etch grooves on the originally smooth free surfaces of the soluble crystals which disappear when removing the stress. Koehn et al. [2004] stressed crystals of NaClO_3 in a NaClO_3 solution at room temperature. Parallel dissolution grooves developed on their free surface in a 1D geometry to a 2D geometry with the coarsening of the pattern. The pressure-solution process slow down or stopped progressively with the increasing concentration of the solution during the experiment. Renard et al. [2001], studied chemical compaction of aggregates of halite (salt) mixed with clay. They showed that clay particles enhance pressure-solution. Moreover, Renard et al. [1997] studied the effect of clay on clay-rich sandstones. Pressure-solution is enhanced by clay because a thick film is preserved between clay particles contrary to between quartz grains. The process is limited by diffusion at great depths, thus at high temperature, as the water film between grains is thin. At low depths, the kinetics limits the process.

The clay particles effect on pressure-solution was recently simulated in numerical modeling. Aharonov and Katsman [2009] used the two-dimensional Spring Network Model to study the stylolites formation in a medium with a uniform clay distribution. They showed that clay plays a role of enhancing pressure-solution and that stylolites propagation is possible only when both pressure-solution and clay-enhanced dissolution operate together. Koehn et al. [2007] developed a new discrete simulation technique that reproduces successfully the roughening of stylolites from a preferential existing surface with no clay. This model is based on molecular dynamics, with a dissolution speed dependent on

the local free energy, including both stress dependent terms and surface energy terms. Two different spatial regimes are observed to arise from this modeling: a small-scale regime where surface energy is dominant with significant fluctuations of the roughness and a large-scale regime where elastic energy dominates. The dependence on the cross-over scale between these two regimes on the imposed stress has been recently investigated numerically Koehn et al. [2012]. This model shows that the growth of the stylolite teeth follows the main compressive stress direction. In this model, the nature and structure of the small scale disorder in the dissolution properties of grains has been systematically analyzed Ebner et al. [2009]. The way in which this disorder reflects the compositional nature of the grains around a stylolite was investigated through detailed microstructural analysis Ebner et al. [2010b].

Stylolites are localised features for which deformation is purely compactant as for compaction bands [Mollema and Antonellini, 1996; Baud et al., 2004; Katsman et al., 2006b]. Stylolites and compaction bands development was modeled as anticracks or anti-mode I fracture [Fletcher and Pollard, 1981; Rispoli, 1981; Mollema and Antonellini, 1996]. Fletcher and Pollard [1981] suggest that the rate of pressure-solution is only a function of the normal stress. They observed an elliptic dissolution pattern i.e. more dissolution in the central part of the stylolites than at the tips. The higher stress concentration at the top of the teeth is responsible of this localised high rates of dissolution. With these observations they proposed an analogy between propagation of stylolites and propagation of mode I fractures. The stress concentrates at the tips and is perpendicular to the stylolite. However, in their simulations of localised volume loss for defects as stylolites, Katsman et al. [2006a] show that the stress is not as enhanced at the tips of the stylolites as for cracks, and depends on the amount of volume removed: they showed that the stress perturbation around a stylolite with a constant volume reduction is analogous to the one around a dislocation, rather than one of a crack. In later models Katsman et al. [2012], if accumulation of dissolution is allowed for in the center of a stylolite, due for example to a positive feedback for the reaction rate induced by clay accumulation, the dissolution profile can become inhomogeneous in models, and then another type of stress enhancement, closer to a crack one, can be observed.

Many studies were conducted on the morphology of sedimentary stylolites [Renard et al., 2004; Brouste et al., 2007; Ebner et al., 2008, 2010a]. Morphology analysis can be done on 1D profiles or 2D opened surfaces. It consists on studying a stylolitic profile or surface variations (standard deviation, height differences, power spectrum, average wavelet coefficient spectrum, etc.) over different scales [Schmittbuhl et al., 1995, 2004; Renard et al., 2004]. These analysis reveal two distinct scaling regimes that could be described by power laws. The power laws are function of a roughness exponent also called Hurst exponent inferred to be 1 and 0,5 for small and large-scale respectively [Renard et al., 2004; Schmittbuhl et al., 2004; Brouste et al., 2007; Ebner et al., 2008]. The two regimes are separated by a cross-over length typically around 1 mm [Renard et al., 2004; Schmittbuhl et al., 2004]. For sedimentary stylolites, the two dimensional (2D) analysis of the surface of stylolites, or the analysis of profiles extracted at different directions, in most cases, does not show any significant inplane anisotropy, reflecting the fact that horizontal stresses are isotropic.

Ebner et al. [2010a] observed that tectonic stylolites profiles show the same geometric attributes as sedimentary ones. Two different regimes are also observed with Hurst exponent around 1 and 0,5 for small and large-scale respectively. However, for tectonic stylolites, the 2D analysis revealed an anisotropy of the cross-over length which varies with the direction in the plane of the stylolites. Ebner et al.

[2010a] explain this anisotropy, i.e. the variation of the cross-over with inplane direction by the way of formation of the stylolites in an anisotropic inplane stress: the vertical and inplane horizontal stress components are significantly different.

Interfaces between solid and fluids are related to models of stylolitization. In the case where a solid in contact with a fluid is stressed, an instability due to pressure solution has been shown theoretically to exist, named the Asaro Tiller Grienfeld (ATG) instability *Renard et al.* [2004]. In models of dissolving surfaces with a stress imposed to a solid in contact with a fluid at chemical equilibrium, this instability leads to the growth of initial large scale modulations of the surface, with a wavelength selection obtained through a fastest growing mode. The basic equation depends on the particular boundary conditions. e.g., when two solids with different elastic properties are in contact and submitted to a stress, the interface can undergo a fingering instability led by the contrast between the free energies in the two solids *Angheluta et al.* [2008]; *Angheluta et al.* [2009, 2010]. Technically, the stability analysis can be performed theoretically from expressions for the kinetics using local free energy criteria for the reaction rate *Renard et al.* [2004]; *Schmittbuhl et al.* [2004], or global ones *Bonnetier et al.* [2009]; *Angheluta et al.* [2008]. Depending on the boundary conditions, this situation is also found to be unstable for perturbations exceeding a certain wavelength, leading to fingering (as e.g. with large stress tangential to a fluid interface *Renard et al.* [2004], or a stress normal to fluid interfaces and lateral periodic boundary conditions *Bonnetier et al.* [2009]). With other boundary conditions, the surface energy and elastic interactions are found to stabilize the interfaces, which are only destabilized by material noise due to heterogeneities *Schmittbuhl et al.* [2004]; *Koehn et al.* [2007]. We will argue in details in the discussion section about the different possibilities applied to the geometry of stylolites, and the fact that stylolites displaying self affine scaling laws for their height at large scale are compatible with the stabilizing character of elastic forces at large scale.

The existence of two scaling regimes for sedimentary stylolites has been shown in *Schmittbuhl et al.* [2004]. A brief theoretical derivation has been performed in this work, that showed that the cross over length between the two scaling regime is expected to be dependent on the stress acting on the stylolite during its formation. It was then concluded that stylolite morphology can be used as a paleostress magnitude indicator. In the current manuscript, we will derive the details of the computation leading to this link between paleostress magnitude and the crossover length between the two scaling regime. We will thus establish the precise link between formation stress and crossover magnitude. This will be performed in section 2, by a perturbative analysis of the elastic energy around an interface slightly wavy and unaligned with one of the principal stresses. We will then show in section 3 that the mechanics and chemistry allows to relate the small scale behavior and large scale behavior of stylolites to known models, with Hurst exponents corresponding to the observed ones. We will eventually show on natural examples in the Bure-sur-Meuse carbonates, how the predicted scaling regimes can be found, and how to reconstruct the magnitude of paleostress at the time of formation of the stylolites, from the determination of the crossover length.

Since this work was first shown in *Schmittbuhl et al.* [2004], independent determinations of the link between cross over length scales and the formation stress were obtained: one on field studies *Ebner et al.* [2008], where the stress derived from the application of this model, and the one inferred from the stylolite depth, were found to be in accordance. Another one, based on numerical simulations of molecular dynamics *Koehn et al.* [2012], also lead to the same relation between imposed stress and crossover scale.

2. Continuous elastostatic model for stylolite formation

The morphology of stylolites arises from the disorder present in a rocks material properties, expressed in the pressure dissolution process.

This disorder is spatially attached to the grains constituting the rock. To understand the impact of this disorder on the chemico mechanical coupling, we will consider the following simplified geometrical scenario: the stylolite is modeled as an elongated fluid pocket, enclosed between two rough surfaces. The stress in the rock, far away from this pocket, is referred to as σ^0 . The direction of the largest principal stress axis is referred to as the z -axis. The large scale average direction of both embedding surfaces is assumed to be perpendicular to z , as observed normally for stylolites. In order to describe elongated fluid pockets, we simplify the geometry as a pocket embedded between two contactless surfaces of infinite extent. Contacts between these two surfaces can in principle modify the geometry of the resulting dissolution surface, but they are assumed to be sufficiently loose in a real stylolite, so that the main morphological results are not affected by them. Notably, we will see that the low-scale and large scale self affine character of the dissolution surfaces, together with the two associated roughness exponents, are well reproduced with the present assumptions, i.e. that the current model leads to the experimentally observed exponents [*Schmittbuhl et al.*, 2004].

In order to have better statistics on the morphology of the surfaces studied, the model is assumed to be symmetric under translation along a y -axis, lying within the average stylolite plane. We describe therefore a two dimensional model. This restriction will allow to describe a larger range of scales at identical same numerical cost, and to resolve numerically the self-affine character of the resulting pressure dissolution surfaces over a larger number of decades. Note however that no particular difficulty is associated with taking into account the third dimension, which can be included straightforwardly using the same approach. Since we first

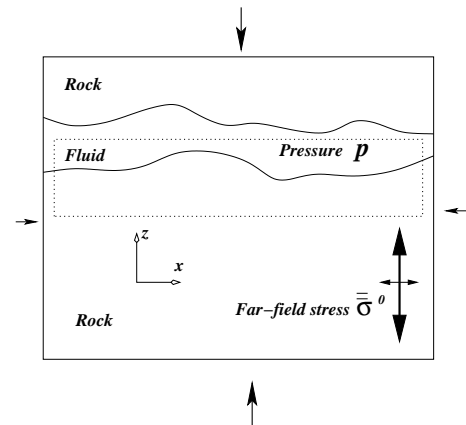


Figure 1. Trapped elongated fluid pocket

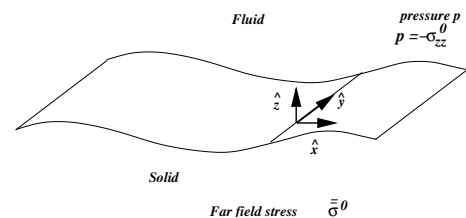


Figure 2. Solid-fluid interface: geometry considered

neglect the solid contacts between the opposite surfaces, the dissolution process happening on both surfaces (figure 1 can be described by the same model, describing the dissolution of a solid half-plane in contact with a fluid half-plane. The basis of the model consists in assuming mechanical equilibrium throughout the system, and in relating the dissolution rate to the stress tensor, and to the area of the interface per unit volume.

2.1. Force perturbation related to the mechanical equilibrium along the fluid-solid interface

First, the mechanical equilibrium at the solid-fluid interface (figure 2) is expressed:

The pressure in the fluid is homogeneous. Since the fluid pocket transmits all the load through it, the fluid pressure is equal to the largest principal stress in the solid, far from the pocket:

$$p = -\sigma_{zz}^0 \quad (1)$$

where by convention, negative stresses represent compressive forces. This equation can be obtained, e.g., by considering the integral of the local stress field σ along an elongated rectangular boundary (dashed line in figure 1).

Next, the mechanical equilibrium is expressed locally, along the interface. The local stress σ is separated between the far-field asymptotic value σ^0 and a perturbation generated by the irregular character of the interface, σ^1 :

$$\sigma(x) = \sigma^0 + \sigma^1(x) \quad (2)$$

The unit vector \hat{n} normal to the surface pointing towards the fluid, is assumed to be close to the principal stress axis. The interface is described as a monovalued function $z(x)$, and we assume slopes of order ϵ , i.e. that $|\partial_x z| \in O(\epsilon) \ll 1$.

The following derivation will be done within such small-angle deviation from a straight surface, and will thus be valid for small surface slopes. The model derived is expected to describe well the onset of the stylolite formation from a flat surface, and we expect it also to hold to describe the evolution of large wavelength modes, since the aspect ratio of such modes (ratio of the amplitude over the wavelength) will be found to be small, corresponding to small effective slopes at large wavelength.

In this limit, requiring $\hat{n} \cdot (1, \partial_x z)^T = 0$, and $\hat{n}^2 = 1$, we find to leading order in ϵ that

$$\hat{n} = \hat{z} - (\partial_x z)\hat{x} + O(\epsilon^2) \quad (3)$$

The far field stress admits \hat{x} and \hat{z} – the units vectors along the z and x axis – as principal directions, i.e.

$$\sigma^0 = \sigma_{xx}^0 \hat{x}\hat{x} + \sigma_{zz}^0 \hat{z}\hat{z} \quad (4)$$

For a stylolite, the most compressive stress axis is normal to the average fluid pocket direction, i.e.

$$|\sigma_{zz}^0| > |\sigma_{xx}^0| \quad (5)$$

We will see straightforwardly that this has strong implications on the stability of the surface patterns emerging from the dissolution process.

We define the far field applied deviatoric stress as

$$\sigma_s^0 = (|\sigma_{zz}^0| - |\sigma_{xx}^0|) = (\sigma_{xx}^0 - \sigma_{zz}^0) \quad (6)$$

The local mechanical equilibrium is expressed at the fluid-solid interface, i.e.

$$\sigma \cdot \hat{n} = -p\hat{n} \quad (7)$$

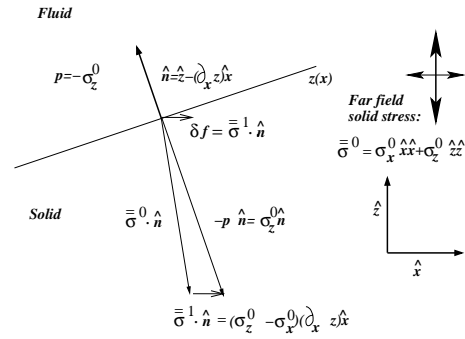


Figure 3. Local mechanical equilibrium along the fluid-solid interface

which together with Equations (1-6), leads to the following expression for the force perturbation related to the curved character of the interface:

$$\begin{aligned} \delta f(x) &= \sigma^1(x) \cdot \hat{n} = \\ &= -p\hat{n} - \sigma^0 \cdot \hat{n} \\ &= \sigma_{zz}^0 [\hat{z} - (\partial_x z)\hat{x}] - \sigma_{zz}^0 \hat{z} + \sigma_{xx}^0 (\partial_x z)\hat{x} \\ &= (\sigma_{xx}^0 - \sigma_{zz}^0) (\partial_x z)\hat{x} \\ &= \sigma_s^0 (\partial_x z)\hat{x} \end{aligned} \quad (8)$$

This force balance is illustrated in Figure 3.

2.2. Chemico-mechanical coupling

Next, we have to express the chemico-mechanical coupling. The dissolution rate of the solid into the fluid, or dissolution speed normal to the solid/fluid interface, is to first order proportional to the chemical potential $\Delta\mu$ of the chemical product dissolving:

$$v = m\Delta\mu \quad (9)$$

where

$$m = k_0\Omega/RT \quad (10)$$

is the mobility of the dissolving specie [Kassner *et al.*, 2001]. Here, $R = 8.31 \text{ J.mol}^{-1}.\text{K}^{-1}$ is the universal gas constant, T the temperature in Kelvins, k_0 is a dissolution rate, which can be assessed experimentally, and Ω is a molar volume. For example, for calcite, $\Omega \simeq 4 \cdot 10^{-5} \text{ m}^3.\text{mol}^{-1}$, and for a dissolution of calcite in water, $k_0 \simeq 10^{-4} \text{ mol.m}^{-2}.\text{s}^{-1}$. The chemical potential drop from the solid to the fluid state, is

$$\Delta\mu = \Delta\Psi_s + \Omega\Delta P_n + \Omega\gamma\kappa \quad (11)$$

In the above, Ω is a molar volume. Considering a solid state at a given pressure and elastic free energy, in chemical equilibrium with the fluid, $\Delta\Psi_s$ and ΔP_n are defined respectively as the change in Helmholtz free energy per mole and the change in stress normal to the interface, with respect to this state. The last term represents the surface energy, with $\kappa = \partial_{xx}z$ the surface curvature (the inverse of the radius of curvature), and γ the surface tension between the solid and fluid phase. Neglecting effects due to temperature variations, and assuming that the fluid composition is in chemical equilibrium with a solid at normal pressure p and stress σ^{ref} , we have $\Delta P_n = 0$ and

$$\Delta\Psi_s + \Omega\Delta P_n = \Omega\Delta u_e, \quad (12)$$

where

$$u_e = [(1 + \nu)\sigma_{ij}\sigma_{ij} - \nu\sigma_{kk}\sigma_{ll}]/4E \quad (13)$$

is the elastic free energy per unit volume, with E the Young modulus and ν the Poisson ratio of the elastic solid, and

$$\Delta u_e = u_e(\sigma) - u_e^{ref} \quad (14)$$

To take into account the dissolution speed variations associated to the morphology, we develop the dissolution rate to leading order as

$$v = v^0 + v^1 \quad (15)$$

and from the above,

$$\begin{aligned} v^0 &= \frac{k_0 \Omega^2}{RT} \left(\frac{[(1+\nu)\sigma_{ij}^0 \sigma_{ij}^0 - \nu \sigma_{kk}^0 \sigma_{ll}^0]}{4E} - u_e^{ref} \right) \\ &= \frac{k_0 \Omega^2}{RT E} (\alpha p_0^2 - \alpha_{ref} p_{ref}^2) \end{aligned} \quad (16)$$

where the following geometrical factor is computed assuming $\sigma_{xx}^0 = \sigma_{yy}^0 = -p_0 + \sigma_s/3$, and $\sigma_{zz}^0 = -p_0 - 2\sigma_s/3$:

$$\alpha = \frac{9(1-2\nu) + 2(1+\nu)\sigma_s^2/p_0^2}{12} \quad (17)$$

with a similar expression for α_{ref} characterizing the fluid chemistry, i.e. as function of the pressure and shear stress p_{ref} and σ_s^{ref} of the reference state in chemical equilibrium with the fluid.

Typically, for a limestone with a Young modulus of $E = 8 \cdot 10^{10}$ Pa, under pressures around $p_0 \simeq 10^7$ Pa corresponding to a few hundred meters depth in sedimentary rocks, and for a fluid with a chemical composition in equilibrium with a surface limestone, the order of magnitude of the dissolution speed of such a calcite/water interface is found as:

$$v_n^0 \simeq 10^{-6} \text{ to } 10^{-5} \text{ m.year}^{-1}$$

2.3. Consequences for the stability of the dissolution process

From the local mechanical equilibrium, and the nature of the chemico-mechanical coupling described above, some important considerations can be made about the stability or

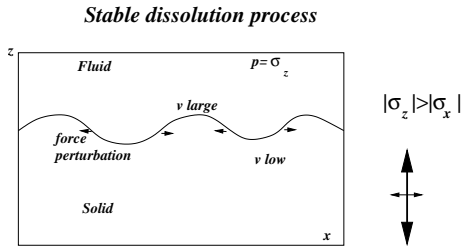


Figure 4. Surface normal to the largest stress axis: stable case

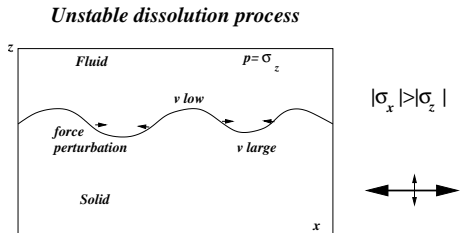


Figure 5. Surface tangential to the largest stress axis: unstable case, Azaro-Tiller-Grinsfeld instability

instability of the shape of dissolution surfaces, depending on the orientation of the interface with respect to the far-field stress.

Indeed, we have shown above that the force perturbation arising from the mismatch between the interface orientation, and the principal axis of the far field stress tensor, \hat{x} , can be expressed from Equation (8), as

$$\delta f(x) = \sigma_s^0 (\partial_x z) \hat{x}$$

This holds independently of the relative magnitude of the principal stresses, σ_{xx} and σ_{zz} . If the largest principal stress is tangential to the interface – which is not the case for stylolites –, $\sigma_s^0 < 0$, and $\delta f(x) \cdot \hat{x}$ has a sign opposite to the interface slope $\partial_x z$. Such tangential force perturbation is concentrated on the points lying ahead of the average dissolution front – on the valleys of this figure, where the dissolution propagates downwards – (figure 5). Thus, the elastic forces will concentrate stress in this points, and the free energy will be higher there, leading to an increased dissolution speed for the points lying already ahead of the average front. The opposite conclusion can be done for the points lying behind of the average front, in the crests of Figure 5, where the dissolution will be slowed down, thus leading them further from the average front. So, the points lying out of the average dissolution plane will tend to depart further to the average position, and the long range elastic forces are a destabilizing force in this situation. On contrary, the surface tension tends to lower the interface area, and to flatten the interface, i.e. stabilizes the process.

The competition between the elastic long-range elastic forces and the surface tension short range stabilizing forces lead to an interface instability known as the Azaro-Tiller-Grinsfeld instability. The wavelength growing fastest in this case is determined by the balance between this long-range destabilizing, and short range stabilizing effects. This instability arising in stressed solids has been studied theoretically [Misbah et al., 2004; Asaro and Tiller, 1972; Grinfeld, 1986], and observed experimentally [Den Brok and Morel, 2001; Koehn et al., 2004].

Conversely, if the largest principal stress lies perpendicular to the interface, as is the case for stylolites, $\sigma_s^0 > 0$, and $\delta f(x) \cdot \hat{x}$ has the same sign as the interface slope $\partial_x z$. Such tangential force perturbation is concentrated on the points lying behind the average dissolution front – on the crests of this figure, where the dissolution propagates downwards – (figure 4). Thus, the elastic forces will concentrate stress in this points, and the free energy will be higher there, leading to an increased dissolution speed for the points lying behind the average front. The opposite conclusion can be done for the points lying ahead of the average front, in the valleys of Figure 4. So, the points lying out of the average dissolution plane will tend to come back to the average position, and the long range elastic forces are a stabilizing force in this situation.

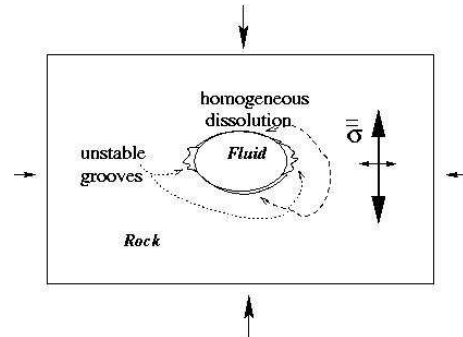


Figure 6. Expected stability or instability of the dissolution front around a trapped fluid pocket

Here as well, the surface tension stabilizes the process.

Consequently, since both the long-range elastic and the short range surface tension forces are stabilizing forces, if the solid properties are modeled as purely homogeneous ones (i.e. a homogeneous elastic solid, with homogeneous dissolution rate properties), this model predicts that any initial non-plane surface will tend to flatten after some time.

So, in order to model the morphogenesis of stylolites, which are rough surfaces normal to the largest stress axis, the disorder attached to material properties has to be taken into account.

2.3.1. Consequence on initial evolution of trapped fluid pocket

The above arguments show that in summary, an elementary bump of a flat surface disappears for $\sigma_s > 0$, or grows for $\sigma_s < 0$. Qualitatively, if this argument on the stability of surfaces depending on their orientation on the principal stress axis extends for more local orientations along trapped fluid pockets, one should observe the following: for the sides of a fluid pocket lying tangentially to the largest stress, these should develop insalable grooves penetrating into the solid, similarly to the ATG instability case. On contrary, the sides normal to the largest stress direction should remain relatively flat, apart from the fluctuations due to the disorder. This small variations along the surfaces normal to the principal stress axis, and penetration in grooves of characteristic wavelength the rock in the directions along the weakest stress, should lead to the development of elongated structures, and merge initially separated fluid pockets (or clay enriched pockets). This qualitative mechanism is illustrated on Fig. 6. This expectation of qualitative evolution is indeed compatible with the mechanism development of anti-cracks, numerically obtained by [Koehn *et al.*, 2003]. The experimental grooves observed along the free surface on the sides of a fluid filled cylindrical pocket, by [Den Brok and Morel, 2001], also displayed this tendency.

2.4. Expression of the dissolution speed perturbation as function of the interface shape

To take into account the disordered nature of the solid, we assume that the material properties, attached to the grains, vary in a random and spatially uncorrelated way. For example, the dissolution constant k is modeled as an average term k_0 , plus a spatially varying one of zero average, $\eta(x, z) \cdot k_0$:

$$k = k_0(1 + \eta(x, z(x))) \quad (18)$$

The random variable η is a quenched disorder without spatial correlations, and is characterized by its average $\langle \eta \rangle = 0$, and its variance $\langle \eta^2 \rangle$, assumed small to keep small local slopes. From Equations(9,15), the dynamics of the dissolving interface $z(x, t)$ can be described as

$$\partial_t z(x, t) = -v_0 - v_1(x, t) \quad (19)$$

with a homogeneous dissolution speed v_0 given by Equation (16), and a deviation v_1 of the dissolution speed with respect to the average dissolution speed v_0 , expressed as:

$$\begin{aligned} v^1 = & \frac{k_0 \Omega^2}{RT} \frac{(\alpha p_0^2 - \alpha_{ref} p_{ref}^2)}{E} \eta(x, z(x)) \\ & + \frac{k_0 \Omega^2}{RT} \gamma \partial_{xx} z(x) \\ & + \frac{k_0 \Omega^2}{RT} \left(\frac{[(1 + \nu) \sigma_{ij}^0 \sigma_{ij}^1 - \nu \sigma_{kk}^0 \sigma_{ll}^1]}{2E} \right) \end{aligned} \quad (20)$$

where σ^1 is the stress perturbation generated in the solid by the surface distribution of tangential force perturbations $\delta f(x)$ associated to the curved character of the interface, derived in Equation (8).

The first term is a quenched disorder term leading the roughening of the interface, the second one is a stabilizing quadratic short ranged term arising from the interfacial tension. The last term can be expressed via a nonlocal kernel from the shape of the interface $z(x)$, by integrating the elastostatic equations in the solid half-plane.

2.5. Detailed form of the elastic long-range interaction kernel

The stress perturbation induced by the force distribution $\delta f(x) = \sigma_s^0(\partial_x z)\hat{x}$ exerted along the surface can be determined via the Green function method: the displacement induced by an elementary force \hat{x} exerted at the origin $(0, 0, 0)$ on a semi infinite solid, is, according to Landau and Lifschitz [Landau and Lifschitz, 1986]:

$$\begin{aligned} a_x(x, y, z) &= \frac{1 + \sigma}{2\pi E} \left\{ \frac{2(1 + \sigma)r + z}{r(r + z)} + \frac{(2r(\sigma r + z) + z^2)}{r^3(r + z)^2} x^2 \right\} \\ a_y(x, y, z) &= \frac{1 + \sigma}{2\pi E} \left\{ \frac{2r(\sigma r + z) + z^2}{r^3(r + z)^2} xy \right\} \\ a_z(x, y, z) &= \frac{1 + \sigma}{2\pi E} \left\{ \frac{(1 - 2\sigma)x}{r(r + z)} + \frac{zx}{r^3} \right\} \end{aligned} \quad (21)$$

From this expression, the associated strain (at points different from the origin) is obtained as

$$\epsilon_{ij}^e = \frac{1}{2}(\partial_i a_j + \partial_j a_i) \quad (22)$$

and the associated stress as

$$f_{ij}(x, y, z) = \frac{E}{1 + \nu} (\epsilon_{ij}^e + \frac{\nu}{1 - 2\nu} \epsilon_{kk} \delta_{ij}) \quad (23)$$

The stress associated to the point force \hat{x} exerted on the surface of normal \hat{z} at the origin, is equal at the origin itself to $\hat{x}\hat{z} + \hat{z}\hat{x}$.

Since the model treated here is invariant by translation along y , the force perturbation $\delta f(u) = \sigma_s^0(\partial_u z)(u)\hat{x}$ is exerted at any $y \in] - \infty, \infty[$ and the resulting stress on the surface, at $(x, y, z = 0)$, is solely dependent on x and can be expressed, by linearity of the elastostatics equations, as

$$\begin{aligned} \sigma_{ij}^1(x) = & \sigma_s^0 \cdot p.p. \left[\int_{x'=-\infty}^{\infty} du (\partial_u z)(u) \int_{y=-\infty}^{\infty} f_{ij}(x - u, -v, 0) dv \right] \\ & + \sigma_s^0(\partial_x z)(x) (\delta_{ix} \delta_{jz} + \delta_{iz} \delta_{jx}) \end{aligned} \quad (24)$$

where p.p. refers to the principal part of the integral. Taking the derivatives of the elementary displacement field in Equation (22), summing to obtain the associated stress, and integrating along the y -axis, comes

$$\int_{y=-\infty}^{\infty} f_{ij}(x, -v, 0) dv = -\frac{2\nu}{\pi x} (\delta_{ix} \delta_{jx} + \delta_{iy} \delta_{jy}) \quad (25)$$

and thus,

$$\begin{aligned} \sigma^1(x) = & -\frac{2\nu \sigma_s^0}{\pi} \cdot p.p. \left[\int_{x'=-\infty}^{\infty} du \frac{(\partial_u z)(u)}{x - u} \right] (\hat{x}\hat{x} + \hat{y}\hat{y}) \\ & + \sigma_s^0 \cdot (\partial_x z)(x) (\hat{x}\hat{z} + \hat{z}\hat{x}) \end{aligned} \quad (26)$$

Together with the expression

$$\sigma^0 = -(p_0 - \sigma_s^0/3)(\hat{x}\hat{x} + \hat{y}\hat{y}) - (p_0 + 2\sigma_s^0/3)\hat{z}\hat{z} \quad (27)$$

the elastic energy perturbation associated to the interface deformation can be computed as

$$\begin{aligned} u_e^1 &= \frac{[(1 + \nu)\sigma_{ij}^0\sigma_{ij}^1 - \nu\sigma_{kk}^0\sigma_{ll}^1]}{2E} \\ &= \frac{2\nu[(1 - 2\nu)p_0 - (1 + \nu)\sigma_s^0/3]}{\pi E} \sigma_0^s \cdot \\ & p.p. \left[\int_{u=-\infty}^{\infty} du \frac{(\partial_u z)(u)}{x - u} \right] \end{aligned} \quad (28)$$

2.6. Dynamic equation for the dissolution interface

From Equations (19, 6, 28), the equation ruling the interface dissolution dynamics is $\partial_t z(x, t) = -v^0 - v^1(x, t)$, with v^0 given by Equation (16), and:

$$\begin{aligned} \frac{RT}{k_0\Omega^2} v^1 &= \frac{(\alpha p_0^2 - \alpha_{ref} p_{ref}^2)}{E} \eta(x, z(x)) \\ & - \gamma \partial_{xx} z(x) \\ & + \beta \frac{p_0 \sigma_s^0}{E} \cdot \\ & p.p. \left[\int_{u=-\infty}^{\infty} du \frac{(\partial_u z)(u)}{x - u} \right] \end{aligned} \quad (29)$$

with a geometrical factor

$$\beta = [2\nu(1 - 2\nu) - (1 + \nu)\sigma_0^s/p_0]/\pi \quad (30)$$

A dimensionless form of this equation can be obtained by adopting length and time units as

$$L^* = \gamma E / (\beta p_0 \sigma_s) \quad (31)$$

$$\tau = (L^*)^2 RT / (\gamma k_0 \Omega^2) \quad (32)$$

and defining the dimensionless variables, in the reference frame moving at the average velocity $-v_0$, as

$$z' = [z + (v_0 t)] / L^* \quad (33)$$

$$x' = x / L^* \quad (34)$$

$$t' = t / \tau \quad (35)$$

and the reduced quenched noise as

$$\eta'(x', z'(x, t) - v_0 t / L^*) = [(\alpha p_0^2 - \alpha_{ref} p_{ref}^2) / (\beta p_0 \sigma_s)] \eta(x, z(x, t)) \quad (36)$$

The dimensionless stochastic equation for the pressure dissolution process is then:

$$\partial_{t'} z'(x', t') = \quad (37)$$

$$\begin{aligned} & \eta'(x', z'(x', t') - v_0 \tau t' / L^*) + \partial_{x' x'} z' \\ & - p.p. \left[\int_{u=-\infty}^{\infty} du \frac{(\partial_u z')(u)}{x' - u} \right] \end{aligned} \quad (38)$$

At large average dissolution speed, the term $v_0 \tau t' / L^*$ dominates quickly over z' , and the noise is annealed – mainly dependent on time, rather than on space. On contrary, for processes sufficiently slow such as the roughness of the surface extends over several grains of disorder, i.e. such as the variation of η' arising from $z'(x', t')$ dominates over the one coming from the average dissolution front position in the solid, $v_0 \tau t' / L^*$, the noise can be considered as quenched, i.e. in first order, the noise dependence is mainly $\eta'(x', z'(x', t'))$. This is the case of interest here, and the dynamic equation can then be cast as

$$\partial_{t'} z'(x', t') = \quad (39)$$

$$\eta'(x', z'(x', t')) + \partial_{x' x'} z' - p.p. \left[\int_{u=-\infty}^{\infty} du \frac{(\partial_u z')(u)}{x' - u} \right] \quad (40)$$

Alternatively, in arbitrary spatial units ℓ , this can also be written

$$\begin{aligned} \partial_t z(x, t) &= \eta''(x', z'(x', t')) + \partial_{xx} z \\ & - \frac{\ell}{L^*} \int dy \frac{\partial_y z}{x - y} \end{aligned} \quad (41)$$

with $L^* = \gamma E / (\beta p_0 \sigma_s)$, and $\tau = \ell^2 RT / (\gamma k_0 \Omega^2)$: time unit.

2.7. Small and large scale behavior of the model

In the small scale limit, for scales $l \ll L^*$, elastic interactions can be neglected in Equation (41), and this model reduces to a Laplacian description:

$$\partial_t z'(x, t) = \partial_{xx} z' + \eta(x, z'(x)) \quad (42)$$

This is known as the Edwards Wilkinson model [Edwards and Wilkinson, 1982], modified with a quenched random noise. This system has been studied in the literature, and leads to the growth of self-affine surfaces of roughness $\zeta \sim 1.2$ [Roux and Hansen, 1994], in agreement with the observation of natural stylolites ($\zeta \sim 1.1$) [Schmittbuhl et al., 2004].

Conversely, in the large scale limit, i.e. for scales $l \gg L^*$, surface tension can be neglected and this Equation (41) reduces to a mechanical regime:

$$\partial_t z'(x, t) = -\frac{\ell}{L^*} \int dy \frac{\partial_y z}{x - y} + \eta(x, z'(x)) \quad (43)$$

Once again, this model is isomorphic to known models for the propagation of an elastic line on a disordered pinning landscape, or for mode I fracture front in a disordered solid. This leads to the growth of self affine surfaces of roughness $\zeta \simeq 0.5$ [Tanguy et al., 1998].

Thus, the model derived above is expected to lead to the growth of dissolution surfaces with self affine characteristics at small scales with $\zeta_1 \sim 1.2$, and a cross over around L^* to display a large scale self affinity with $\zeta_2 \sim 0.5$.

3. Numerical approach

The above shows from a purely analytical point of view, via isomorphisms of the asymptotic small scale equations version and of the large scale equations version to know models, that two different scaling laws are expected for small and large scales, and that the cross over should depend on the far field stress magnitude. Independently from this general analytical analysis, we will now show how to solve for this model numerically, i.e. implement the dynamic evolution of evolution of the interface with all the large and small scale terms and random variables to represent the disorder, and analyse the resulting morphogenesis.

3.1. Practical implementation of the model

We simulate the dissolution process for a calcite water interface with constants identical to the ones used in the discrete lattice code, i.e.: Surface tension $\gamma = 0.35 J \cdot m^{-2}$, molecular volume $2.2688 \cdot 10^{-5} m^3/mol$, elastic properties of the modeled rock: Poisson ratio $\nu = 0.33$, Youngs modulus $E = 40$ Gpa, Dissolution rate $k_0 = 10^{-7} mol \cdot m^{-2} \cdot s^{-1}$. The physical conditions adopted correspond to a temperature $T = 420$ K, and average stresses p and σ_s around 10 to 40 MPa.

For the amount of the quenched noise associated to the natural variations of the grain properties, the typical scale attached to the quenched disorder (or typical grain size) is considered to be around $\ell = 10\mu\text{m}$ – with no correlations above this scale –, and the quenched disorder is characterized by a standard deviation $\sqrt{\langle \eta^2 \rangle} = [\alpha \ell p_0 / (\beta L^* \sigma_s)] \cdot [(\delta E/E) + (\delta k/k_0) + (\delta \alpha/\alpha)]$ corresponding to relative variations of the dissolution rate of order 10% (i.e. $\delta k/k_0 \sim 0.1$).

The dimensionless surface dynamic equation, without disorder, would be:

$$\partial_t z(x, t) = v_0 + \partial_{xx} z - \frac{\ell}{L^*} \int dy \frac{\partial_y z}{x-y} \quad (44)$$

where $L^* = \gamma E / (\beta p_0 \sigma_s)$, ℓ is the unit length, and $\tau = \ell^2 RT / (\gamma k \Omega^2)$ is the time unit.

We assume a small disorder in the implied quantities (e.g. Young Modulus), that are quenched in the material properties of the rock heterogeneity associated with micrometric grains, typically $\ell = 10\mu\text{m}$. The interface is supposed normal to largest stress direction (stabilizing elastic interactions).

By perturbation to first order, in the referential frame of the homogeneously moving average front, $z' = z - v_0 t$, the surface growth equation becomes:

$$\partial_t z'(x, t) = \partial_{xx} z' - \frac{\ell}{L^*} \int dy \frac{\partial_y z'}{x-y} + \eta(x, z(x)) \quad (45)$$

with a quenched random term $\eta(x, z'(x)) = [\alpha \ell p_0 / (\beta L^* \sigma_s)] \cdot [(\delta E/E) + (\delta k/k) - (\delta \alpha/\alpha)]$

Two first terms are stabilizing, only the quenched disorder destabilizes the interface. We perform the simulation of this dynamic equation with both stabilizing terms and quenched noise.

The quantification of the prefactors depend of the rock type, and the formation stress. In addition to these mappings, the characteristic units are known as function of the rock properties. The cross over scale $L^* = \gamma E / (\beta p_0 \sigma_s)$ is function of the pressure during formation, through p_0 and σ_s .

Determining the cross over L^* at lab allows to determine such stress value during formation, and consequently depth of the rock during stylolite formation. Assuming as

Figure 7. Snapshot of the pression-dissolution profile

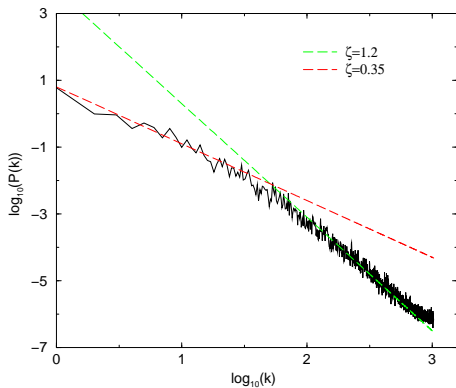


Figure 8. Average power spectrum of simulated stylolitic fronts, in bilogarithmic representation. The k -unit is $2\pi/L$, with $L = 4096\ell$ and a grain size $\ell = 10\mu\text{m}$. The vertical unit is arbitrary. The crossover is obtained at $2\pi/L^*$

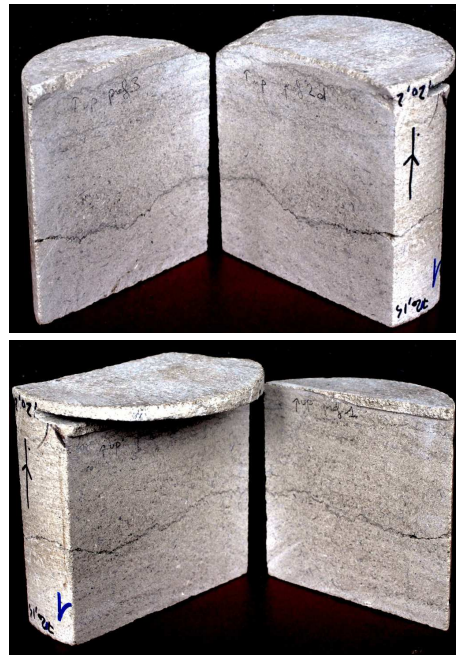


Figure 9. Profiles 1, 2, 3 and 4 from right to left and top to bottom. A core from the Dogger formation (EST433 well) was cut in three parts to obtain four profiles. Each profile was photographed at high resolution.

an order of magnitude $p_0 \sim \sigma_s$ and characteristics values for limestone elastic properties and water calcite reaction rates, $L^* \sim 1\text{mm}$ leads to a typical depth of 1 km. **Stylolites** can thus be considered as **fossils of the stress magnitude**.

The dynamic equation Equation (41) is solved with an event-driven algorithm, where at each step, the fastest dissolving grain is removed. The problem is considered as L -periodic, and consequently the long-range elastic kernel $p.p. \int dy \frac{\partial_y z}{x-y} = -p.p. \int dy \frac{z(x)-z(y)}{(x-y)^2}$ is replaced by its finite-size form, $-p.p. \int_0^L dy \frac{z(x)-z(y)}{\sin^2(\pi(x-y)/L)} \frac{\pi^2}{L^2}$. This classical form can be obtained by solving the elastostatic equations in Fourier space, and performing an inverse Fourier integration. Each time a new grain is reached, the particular realization of its quenched disorder η is evaluated using a Gaussian distribution. The dissolution surface simulated is 4096ℓ long, and 8000000 grains are dissolved.

3.2. Analysis of the small-scale and large-scale roughness of the saturated interface

The simulation of the calcite-water system leads to a grown dissolution interface. Starting from a flat interface, after a transient time, the amplitude of the Fourier modes of these interfaces saturates to a characteristic amplitude. A snapshot of the developed stylolitic interface is shown in Figure 7. This interface fluctuates around the average progressing flat dissolution front. The Fourier power spectrum $P(k, t) = \|\tilde{z}(k, t)\|^2$ of each front $z(x, t)$ is extracted, and the ensemble average of this power spectrum $P(k) = \langle \|\tilde{z}(k)\|^2 \rangle$ is obtained for developed interfaces, by averaging over all fronts after 80000 grains have been dissolved. The expected small and large scale self-affine characteristics correspond to the theoretical expectations, as shown in Figure 8: The power-spectrum is indeed a power-law of scale, with two different exponents at large and small scale, and a cross over around the scale L^* : For $k > 2\pi/L^*$, we have $P(k) \sim k^{-1-2\zeta}$ with $\zeta = 1.2$, and for the large scales, the roughness exponent is found to be around $\zeta = 0.35$. The straight lines in

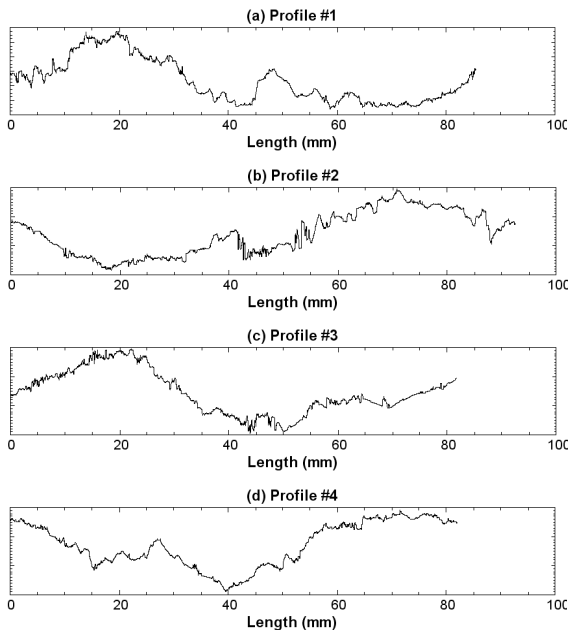


Figure 10. Functions obtained from profiles 1, 2, 3 and 4. A grey-level threshold was imposed on the pictures to isolate the stylolites. The functions were then obtained by selecting the mean of the y coordinate of the pixels belonging to the stylolite, for every x running along the stylolite average.

the bilogarithmic (figure 8) correspond to these Hurst exponents, determined by linear regression over the two domains $k > 2\pi/L^*$ and $k < 2\pi/L^*$.

Thus, we find that the scaling of saturated surfaces in this model is compatible with the laboratory observations, and with the analytical predictions above.

In addition, the dynamic behavior of these models (Edwards Wilkinson in a quenched noise, or elastic string in a disordered landscape) is known. The prefactor (characteristic time) associated with the dynamics can be evaluated through the above from rock material properties. An estimate of time to saturation at an observation scale of a few centimeters is around a few thousands of years: the stylolite roughness is hence always at saturation value for a geologist at small observation scales.

However, for longer systems, e.g. decametric ones, much longer times would be required for saturation. Such long stylolites are sometimes observed but seldom analysed in terms of scaling of the height. In the only long case studied to our knowledge, it was found that the large scales are not saturated [Laronne Ben-Itzhak et al. [2012b]]. This means that the time during which the stylolitisation was active on such very long stylolites was only enough to lead the small scales to saturation amplitude, but not the large ones (above a few tenth of centimeters). The fact that the porosity was clogged by precipitation along these long stylolites probably stopped the evolution.

4. Example: Application of the model on natural data

The model is applied on a stylolite from the ANDRA (French national radioactive waste management agency) Underground Research Laboratory (URL) at Bure in Eastern France. The sample selected comes from the borehole EST433 at a depth of 720 m. The host rock is a fine-grained,

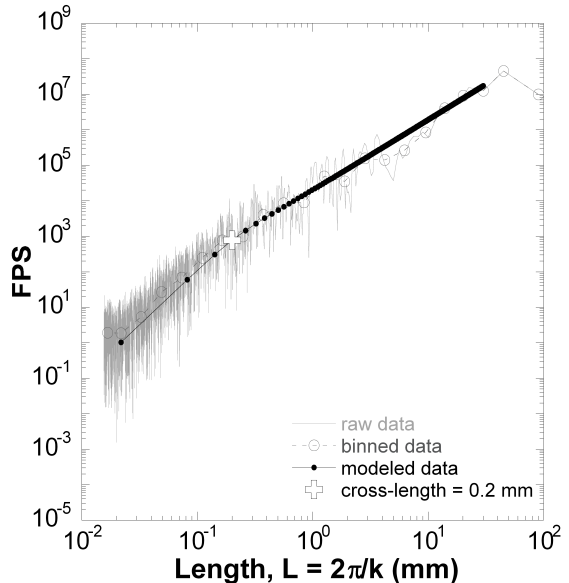


Figure 11. Fourier Power Spectrum of the profile 2. The raw data were binned logarithmically to run a linear-by-part fitting on the data. Two different scaling regimes are observed at small and large scale with Hurst exponent around 1 and 0,5 respectively. The modelled fit reveals a cross-over length L around 0.2 mm.

homogeneous grainstone from the Dogger age. The core was cut in three parts thus giving four profiles for analysis (figure 9). Profiles 1 and 2 and profiles 3 and 4 are spaced by 3 mm (thickness of the drilling saw) and profiles 2 and 3 are spaced by 30 mm. Each profile has a length of 90 mm. The stylolites were photographed at a resolution of $8 \mu\text{m}$. A systematic method was used to extract profiles from the photographs. It consists of isolating the black pixels constituting the clay particles in the stylolite from photographs converted in grey level pictures. The profiles will be used as functions in the spectral analysis (integral transforms) and thus are required to be single-valued. Stylolites show a self-affinity geometry [Schmittbuhl et al., 1995; Barabási and Stanley, 1995] meaning that they are statistically invariant under an affine transformation. Thus, for Δx and Δy the horizontal direction amplitude and Δz the vertical direction amplitude: $\Delta x \rightarrow \lambda \Delta x$, $\Delta y \rightarrow \lambda \Delta y$ and $\Delta z \rightarrow \lambda^H \Delta z$, where λ can take any value and H is the Hurst exponent which describes the scaling invariance. As in Ebner et al. [2008] we used the Fourier Power Spectrum (FPS) [Schmittbuhl et al., 1995] and the Averaged Wavelet Coefficient (AWC) [Simonsen et al., 1998] signal processing methods to analyse the profiles. Other methods can be used such as variable bandwidth methods consisting of calculating the standard deviation or the difference between the maximum and the minimum of the height of the signal [Schmittbuhl et al., 1995]. We used two different methods to repeat the results. First we calculated the Fourier Power Spectrum $P(k)$, which is the square of the modulus of the Fourier transform, as a function of the wave-number k ($k = 2\pi/L$, where L is the wave-length). The power spectrum expressed as a function of the length for a self-affine profile behaves as $P(L) \simeq L^{2H+1}$. We calculated also the averaged wavelet coefficient spectrum with Daubechies 4 wavelets which behaves as $W(a) \simeq a^{1/2+H}$.

Both methods were used to analyze our data (figure 10). The results show the two scaling regimes (see introduction) described by two different power laws. Figure 11 shows the

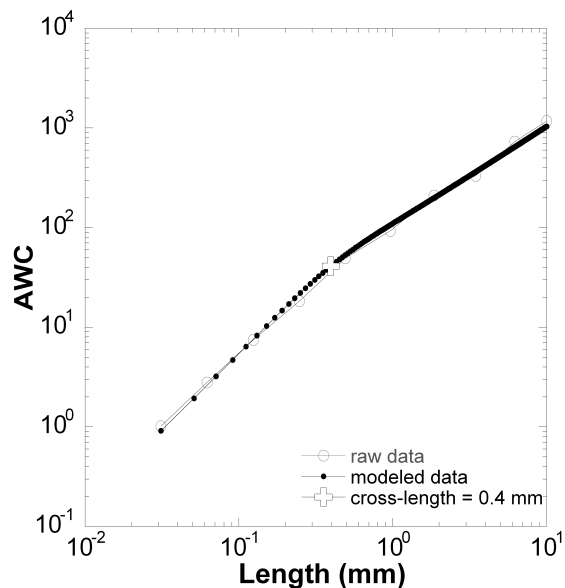


Figure 12. Averaged Wavelet Coefficient spectrum of the profile 2. A linear-by-part fitting were run on the data. Two different scaling regimes are observed at small and large scale with Hurst exponent around 1 and 0,5 respectively. The modelled fit reveals a cross-over length L around 0.4 mm. This is in good accordance with the length estimated with the FPS method.

Fourier power spectrum for the profile 2 as a function of the length L . The raw data are more concentrated at small scale. Indeed, the profiles have a finite-size which gives the upper limit for the analysis (corresponding to small wave-number). To analyze the data, we apply a logarithmic binning so that the weight on each point is equal. To estimate the cross-over length, we used a linear-by-part fit with a crossover function changing the scaling law from small to large scale as explain in *Ebner et al. [2008]*. The averaged wavelet coefficient spectrum (figure 12) doesn't require a binning. The same kind of fitting was used to appraise the cross-over length.

5. Discussion and conclusion

Analysing the local boundary conditions due to the fact that the inside of a stylolite does not sustain shear stress, and an elastic surrounding, we derived the dependence of the free energy along a stylolite surface on the shape of the stylolite. Adding up a surface energy term, we derived a dynamic surface evolution model for a stylolitic interface. This model, in situations where the stylolite is perpendicular to the largest principal stress axis - as is normally the case - was shown to display terms that lead to the stabilization of the surface dynamics, i.e. to the vanishing of initial perturbations towards a flattening surface. Hence, the presence of disorder linked to the heterogeneity of material properties is required to explain the rough character of stylolites. Introducing such non correlated quenched disorder, we obtained that two scaling laws can be predicted: at small scale, a destabilizing disorder competing with a stabilizing surface energy term, leads to a model similar to Edwards Wilkinson model in a quenched noise, which leads to a saturated surface with a Hurst exponent around 1.1. At large scale, the competition of destabilizing disorder, and stabilizing elastic interactions in this configuration, are isomorphic to models of evolution of an elastic interface in quenched disorder, which leads to a Hurst exponent of 0.5.

The cross over scale between these two scaling regime was shown to be directly linked to the stress magnitude. Hence, the determination of this cross over, and other physical properties for a rock, allows to use stylolites as a marker of paleo stress magnitude.

The two scaling laws, and the dependence of this cross over scale on the stress magnitude, had been derived in two ways: by purely analytical derivation and isomorphisms to known models in section 2, and by numerical integration in section 3.

Importantly, it should be noted that the elastic forces, depending on the boundary conditions, can be stabilizing, as here, or destabilizing. The existence of several models, and several techniques of calculations of the free energy, global or local ones, can raise the question of a stabilizing or destabilizing character of the elastic forces in the stylolite context. Apart from the derivation carried out in this article in details, we note the following argument that can distinguish between stabilizing and destabilizing terms: The only difference between models with stabilizing or destabilizing elastic kernel is the sign of the prefactor in front of the elastic operator in the dynamic equation. However, when this sign is reverted, all large scale wavelength Fourier modes become unstable (with a selection of fastest growing mode, as e.g. shown in *Misbah et al. [2004]* or *Bonnetier et al. [2009]*). Numerical simulations similar to the ones shown above, with a destabilizing mode, do not lead to any saturation of the amplitude of the large modes at long times, and the Fourier power spectrum at a given time does not display any scaling law at fixed time for the large scales. Hence, the scaling laws observed in field stylolites are compatible with a model where elastic forces are stabilizing, and not with one where they would be destabilizing: we take this as a good sign of validity of the proposed approximations to take the boundary conditions into account in the proposed model.

In general, the results of these two independent techniques, analytical and numerical ones, are found to be consistent with three other independent observations:

- The existence of two Hurst exponents at small and large scales, as was observed in *Schmittbuhl et al. [2004]*, and as was shown to exist in the stylolites from the log cores of Bure-sur-Meuse in section 4.
- The results of molecular dynamic models of dissolution with pressure dependent and surface energy terms in the free energy, displaying similar scaling laws, and an identical law for the dependence of cross over length over the applied stress *Koehn et al. [2012]*
- The fact that stylolites in a common rock formation in the Cirque de Navacelles, at various depth, show a formation stress derived from this model which is compatible with the derived weight of overburden at the time of formation *Ebner et al. [2008]*

We show eventually on the example of sedimentary stylolites in Bure, how the confinement stress can be derived from morphological studies of stylolites. The ubiquitous character of these pressure solution features makes them a versatile marker for paleostress magnitude, that can give access to the stress at the instant of formation of the stylolites. This easily available paleostress marker opens the way for systematic studies of paleostress in large rock formations of different stylolite families. Together with dating indications for the time of occurrence of such stylolites (as e.g. times of tectonic events), and current stress assessment methods, this opens the way for the determination of stress evolution in large basins, which is a key to understand their evolution.

References

- Aharonov, E., and R. Katsman (2009), Interaction between pressure solution and clays in stylolite development: insights from modeling, *American J. Sci.*, 309, 607–632.

- André, G. (2003), *Caractérisation des déformations méso-cénozoïques et des circulations de fluides dans l'Est du Bassin de Paris*, Thesis, Université Henri Poincaré, Nancy, France.
- Angheluta, L., J. Mathiesen, C. Misbah, and F. Renard (2010), Morphological instabilities of stressed and reactive geological interfaces, *J. Geophys. Res.*, *115*, B06,406.
- Angheluta, L., E. Jettestuen, and J. Mathiesen (2009), Thermodynamics and roughening of solid-solid interfaces, *Phys. Rev. E*, *79*(3, Part 1), doi:10.1103/PhysRevE.79.031601.
- Angheluta, L., E. Jettestuen, J. Mathiesen, and F. Renard (2008), Stress-driven phase transformation and the roughening of solid-solid interfaces, *Phys. Rev. Lett.*, (100), 096,105.
- Asaro, R., and W. Tillier (1972), Interface morphology development during stress-corrosion cracking. 1. Via surface diffusion, *Met. Trans.*, *3*, 1789.
- Barabási, A., and H. Stanley (1995), *Fractal concepts in surface growth*, Cambridge University Press.
- Bathurst, R. G. C. (1971), *Carbonate sediments and their diagenesis*, 620 pp. pp., Amsterdam/London/New York: Elsevier.
- Bathurst, R. G. C. (1987), Diagenetically enhanced bedding in argillaceous platform limestones: stratified cementation and selective compaction, *Sedimentology*, *34*, 749–778.
- Baud, P., E. Klein, and T. F. Wong (2004), Compaction localization in porous sandstones: spatial evolution of damage and acoustic emission activity, *J. Struct. Geol.*, *26*, 603–624.
- Benedicto, A., and R. Schultz (2010), Stylolites in limestones: magnitude of contractional strain accommodated and scaling relationships, *J. Struct. Geol.*, *32*, 1250–1256.
- Bonnetier, E., C. Misbah, F. Renard, R. Toussaint, and J. Gratier (2009), Does roughening of rock-fluid-rock interfaces emerge from a stress-induced instability?, *European Phys. J. B.*, *67*, 121.
- Brouste, A., F. Renard, J. P. Gratier, and J. Schmittbuhl (2007), Variety of stylolites' morphologies and statistical characterization of the amount of heterogeneities in the rock, *J. Struct. Geol.*, *29*, 422–434.
- Bushinskiy, G. I. (1961), Stylolites, *Izv. Akad. Nauk. SSSR, Ser. Geophys.*, *8*, 31–46.
- Buxton, T. M., and D. Sibley (1981), Pressure solution features in a shallow buried limestone, *J. Sediment. Petrol.*, *51*, 19–26.
- Cox, M. A., and J. L. Whitford-Stark (1987), Stylolites in the Caballos Novaculite, West Texas, *Geology*, *15*, 439–442.
- Cox, S. F., and M. S. Paterson (1991), Experimental dissolution-precipitation creep in quartz aggregates at high temperatures, *Geophys. Res. Lett.*, *18*, 1401–1404.
- Den Brok, S. W. J., and J. Morel (2001), The effect of elastic strain on the microstructure of free surfaces of stressed minerals in contact with an aqueous solution, *Geophys. Res. Lett.*, *28*, 603–606.
- Den Brok, S. W. J., and C. Spiers (1991), *J. Geol. Soc. (London)*, *148*, 541.
- D.K., D., F. Renard, J. Feder, B. Jamtveit, P. Meakin, and T. Jssang (2003), High resolution measurements of pressure solution creep, *Phys. Rev. E*, *68*, 011,603.
- Dunnington, H. V. (1954), Stylolite development post-dates rock induration, *J. Sediment. Petrol.*, *24*, 27–49.
- Dysthe, D., Y. Podlchikov, F. Renard, J. Feder, and B. Jamtveit (2002), Universal scaling in transient creep, *Phys. Rev. Lett.*, *89*, 246,102.
- Ebner, M., D. Koehn, R. Toussaint, F. Renard, and J. Schmittbuhl (2008), Stress sensitivity of stylolite morphology, *Earth and Planet. Sci. Lett.*, *277*, 394–398.
- Ebner, M., D. Koehn, R. Toussaint, and F. Renard (2009), The influence of rock heterogeneity on the scaling properties of simulated and natural stylolites, *J. of Struct. Geol.*, *31*, 72.
- Ebner, M., R. Toussaint, J. Schmittbuhl, D. Koehn, and P. Bons (2010a), Anisotropic scaling of tectonic stylolites: a fossilized signature of the stress field, *J. Geophys. Res.*, *115*, B06,403.
- Ebner, M., S. Piazzolo, F. Renard, and D. Koehn (2010b), Stylolite interfaces and surrounding matrix material: Nature and role of heterogeneities in roughness and microstructural development, *J. Struct. Geol.*, *32*, 1070–1084.
- Edwards, S. E., and D. R. Wilkinson (1982), The surface statistics of a granular aggregate, *Proc. R. Soc. London*, *17*.
- Fabricius, I. L., and M. K. Borre (2007), Stylolites, porosity, depositional texture, and silicates in chalk facies sediments. Ontong Java Plateau - Gorm and Tyra fields, North Sea, *Sedimentology*, *54*, 183–205.
- Fletcher, R. C., and D. D. Pollard (1981), Anticrack model for pressure solution surfaces, *Geology*, *9*, 419–424.
- Gratier, J. P. (1993), Experimental pressure solution of halite by an indenter technique, *Geophys. Res. Lett.*, *20*, 1647–1650.
- Gratier, J. P., and R. Guiguet (1986), Experimental pressure solution-deposition on quartz grains: the crucial effect of the nature of the fluid, *J. Struct. Geol.*, *8*, 845–856.
- Gratier, J. P., L. Jenatton, D. Tisserand, and R. Guiguet (2004), Indenter studies of the swelling, creep and pressure solution of Bure argillite, *App. Clay Sci.*, *26*, 459–472.
- Gratier, J. P., L. Muquet, R. Hassani, and F. Renard (2005), Experimental microstylolites in quartz and modeled application to natural stylolitic structures, *J. Struct. Geol.*, *27*, 89–100.
- Grinfeld, M. A. (1986), Instability of interface between nonhydrostatically stressed elastic body and melts, *Sov. Phys. Dokl.*, *31*, 831.
- Heald, M. T. (1955), Stylolites in sandstones, *J. Geol.*, *63*, 101–114.
- Iijima, A. (1979), Nature and origin of the Paleogene cherts in the Setogawa Terrain, Shizuoka, central Japan, *J. Fac. Sci. Univ. Tokyo, Sect. 2*, *20*, 1–30.
- Karcz, Z., E. Aharonov, D. Ertas, R. Polizzotti, and C. H. Scholz (2008), Deformation by dissolution and plastic flow of a single crystal sodium chloride indenter: an experimental study under the confocal microscope, *J. Geophys. Res.*, *113*, B04,205.
- Kassner, K., C. Misbah, J. Müller, J. Kappey, and P. Kohlert (2001), Phase-field modeling of stress-induced instabilities, *Phys. Rev. E*, *63*, 036,117.
- Katsman, R., E. Aharonov, and H. Scher (2006a), A numerical study on localized volume reduction in elastic media: some insights on the mechanics of anticracks, *J. Geophys. Res.*, *111*, B03,204.
- Katsman, R., E. Aharonov, and H. Scher (2006b), Localized compaction in rocks: Eshelby's inclusion and the Spring Network Model, *Geophys. Res. Lett.*, *33*, L10,311.
- Katsman, R., L. Laronne Ben-Itzhak, and E. Aharonov (2012), submitted.
- Koehn, D., J. Arnold, B. Jamtveit, and A. Malthe-Sørenssen (2003), Instabilities in stress corrosion and the transition to brittle failure, *American J. Sci.*, *303*, 956–971.
- Koehn, D., D. K. Dysthe, and B. Jamtveit (2004), Transient dissolution patterns on stressed crystal surfaces, *Geochimica et Cosmochimica Acta*, *68*, 3317–3325.
- Koehn, D., F. Renard, R. Toussaint, and C. W. Passchier (2007), Growth of stylolite teeth patterns depending on normal stress and finite compaction, *Earth and Planet. Sci. Lett.*, *257*, 582–595.
- Koehn, D., M. Ebner, F. Renard, R. Toussaint, and C. Passchier (2012), Modelling of stylolite geometries and stress scaling, submitted.
- Landau, L. D., and E. M. Lifchitz (1986), *Theory of elasticity*, Butterworth-Heinemann-London, 3rd ed.
- Laronne Ben-Itzhak, L., E. Aharonov, and Z. Karcz (2012a), submitted.
- Laronne Ben-Itzhak, L., E. Aharonov, R. Toussaint, and A. Sagy (2012b), Upper bound on stylolite roughness as indicator for the duration and amount of dissolution, submitted.
- Lind, I. L. (1993), Stylolites in chalk from leg 130, Ontong Java Plateau, *Proc. OPD Sci. Results*, *130*, 673–686.
- Misbah, C., F. Renard, J. P. Gratier, and K. Kassner (2004), Dynamics of a dissolution front for solids under stress, *Geophys. Res. Lett.*, *31*, L06,618.
- Mollema, P. N., and M. A. Antonellini (1996), Compaction bands: a structural analog for anti-mode I crack in aeolian sandstone, *Tectonophysics*, *267*, 209–228.
- Park, W. C., and E. H. Schot (1968), Stylolites: their nature and origin, *J. Sediment. Petrol.*, *38*, 175–191.
- Railsback, L. B. (1993), Lithologic controls on morphology of pressure-dissolution surfaces (stylolites and dissolution seams) in Paleozoic carbonate rocks from the mideastern United States, *J. Sed. Res.*, *63*, 513–522.
- Renard, F., P. Ortoleva, and J. P. Gratier (1997), Pressure solution in sandstones: influence of clays and dependence on temperature and stress, *Tectonophysics*, *280*, 257–266.
- Renard, F., D. Dysthe, J. Feder, K. B. Rylke, and B. Jamtveit (2001), Enhanced pressure solution creep rates induced by clay particles: experimental evidence in salt aggregates, *Geophys. Res. Lett.*, *28*, 1295–1298.

- Renard, F., J. Schmittbuhl, J. P. Gratier, P. Meakin, and E. Merino (2004), Three-dimensional roughness of stylolites in limestones, *J. Geophys. Res.*, *109*, B03,209.
- Rispoli, R. (1981), Stress field about strike-slip faults inferred from stylolites and tension gashes, *Tectonophysics*, *75*, 29–36.
- Roux, S., and A. Hansen (1994), Interface roughening and pinning, *J. Phys. I (France)*, *4*, 515–538.
- Rutter, E. H. (1976), The kinetics of rock deformation by pressure solution, *Philos. Trans. R. Soc. London Ser.A*, *283*, 203–219.
- Rutter, E. H. (1983), Pressure solution in nature, theory and experiment, *J. Geol. Soc.*, *140*, 725–740.
- Schmittbuhl, J., F. Schmitt, and C. Scholz (1995), Scaling invariance of crack surfaces, *J. Geophys. Res.*, *100*, 5953–5973.
- Schmittbuhl, J., F. Renard, J. P. Gratier, and R. Toussaint (2004), Roughness of stylolites: implications of 3D high resolution topography measurements, *Phys. Rev. Lett.*, *93*, 238,501.
- Schutjens, P., and C. Spiers (1999), *Oil Gas Sci. Technol.*, *54*, 729.
- Simonsen, I., A. Hansen, and O. M. Nes (1998), Determination of the Hurst exponent by use of wavelet transforms, *Phys. Rev. E*, *58*, 2779–2787.
- Stockdale, P. B. (1922), Stylolites: their nature and origin, *Indiana University Studies*, *9*, 1–97.
- Stockdale, P. B. (1926), The stratigraphic significance of solution in rocks, *J. Geol.*, *34*, 399–414.
- Stockdale, P. B. (1936), Rare stylolites, *American J. Sci.*, *32*, 129–133.
- Stockdale, P. B. (1943), Stylolites: primary or secondary?, *J. Sediment. Petrol.*, *13*, 3–12.
- Stutzer, O. (1940), *Geology of coal*, Univ. Chicago Press.
- Tanguy, A., M. Gounelle, and S. Roux (1998), From individual to collective pinning: Effect of long-range elastic interactions, *Phys. Rev. E*, *58*, 1577–1590.
- Wright, T. O., and L. B. Platt (1982), Pressure dissolution and cleavage in Martingsburg shale, *American J. Sci.*, *282*, 122–135.
- Young, R. B. (1945), Stylolitic solution in Wit-watersrand quartzites, *Geol. Soc. S. Afr. Trans.*, *47*, 137–142.
-
- A. Rolland, Institut de Physique du Globe, Université de Strasbourg, 5 rue René Descartes, 67084 cedex, Strasbourg, FR. (Renaud.Toussaint@unistra.fr)
- R. Toussaint, Institut de Physique du Globe, Université de Strasbourg, 5 rue René Descartes, 67084 cedex, Strasbourg, FR. (alexandra.rolland@unistra.fr)
- P. Baud, Institut de Physique du Globe, Université de Strasbourg, 5 rue René Descartes, 67084 cedex, Strasbourg, FR. (Patrick.Baud@unistra.fr)
- J. Schmittbuhl, Institut de Physique du Globe, Université de Strasbourg, 5 rue René Descartes, 67084 cedex, Strasbourg, FR. (Jean.Schmittbuhl@unistra.fr)
- N. Conil, Agence National pour la gestion des Déchets Radioactifs, Centre de Meuse/Haute-Marne, Route Départementale 960, BP 9, 55290, Bure, FR
- D. Koehn, University of Glasgow
- F. Renard, IsTerre, Université Joseph Fourier, Grenoble
- J.P. Gratier, IsTerre, Université Joseph Fourier, Grenoble